Journal of Applied Physics ARTICLE pubs.aip.org/aip/jap

The role of carbon segregation in the electrical activity of dislocations in carbon doped GaN

Cite as: J. Appl. Phys. **136**, 045704 (2024); doi: 10.1063/5.0213275
Submitted: 9 April 2024 · Accepted: 1 July 2024 ·
Published Online: 23 July 2024

Ze F. Scales,[1,2,a)] Christian Koller,[3] Liverios Lymperakis,[4,5] Michael Nelhiebel,[1] and Michael Stoeger-Pollach[2]

AFFILIATIONS

[1]KAI GmbH, Europastraße 8, Villach 9524, Austria
[2]USTEM, TU Wien, Wiedner Hauptstraße 8-10, 1040 Vienna, Austria
[3]Infineon Technologies Austria AG, Siemensstraße 2, 9500 Villach, Austria
[4]Department of Physics, University of Crete, Voutes University Campus, Heraklion 70013, Greece
[5]Foundation for Research and Technology-Hellas, Institute of Electronic Structure and Laser, Heraklion, Greece

[a)]**Author to whom correspondence should be addressed:** ze.scales@k-ai.at

ABSTRACT

Dislocations have been proposed to affect the performance and reliability of GaN power semiconductors by being conductive pathways for leakage current. However, no direct evidence of a link between their electrical behavior and physical nature in carbon-doped semi-insulating GaN buffer layers has been obtained. Therefore, we investigate the electrical activity of dislocations by conductive atomic force microscopy and electron beam induced current to distinguish electrically active dislocations from non-active ones. We investigated six electrically active dislocations and discovered distinct carbon enrichment in the vicinity of all six dislocations, based on cross-sectional scanning transmission electron microscopy using electron energy loss spectrometry. Electrically non-active dislocations, which are the vast majority, sometimes also showed carbon enrichment, however, in only two out of seven cases. Consequently, carbon segregation seems to be a requirement for electrical activity, but a carbon surplus is not sufficient for electrical activity. We also performed first-principles total-energy calculations for mixed type threading dislocations, which validates carbon accumulation in the dislocation vicinity. The electrical and physical characterization results, complemented by density functional theory simulations, support the previously hypothesized existence of a carbon defect band and add new details.

I. INTRODUCTION

A. Dislocations in GaN-on-Si HEMTs

Electrical energy and efficient power conversion are in high demand globally; therefore, research on gallium nitride (GaN) strives to harness GaN's unique material properties in order to meet these modern technological needs. Remarkably, lateral GaN-on-Si high electron mobility transistors (HEMTs) comprise only a few micrometers of GaN grown on hundreds of micrometers of silicon. Resulting GaN-based devices deliver higher switching frequencies, higher carrier mobilities, and, as a result, more efficient power conversion compared to their silicon-based counterparts.

GaN HEMTs are lateral devices in which the current is constrained to the two-dimensional electron gas (2DEG) a few tens of nanometers below the semiconductor surface. Compared to GaN, the silicon substrate is relatively conductive and, consequently, has to be electrically isolated from vertical leakage currents between the 2DEG and the substrate to prevent performance losses in OFF state and charge trapping. Most commonly, this is achieved by doping the GaN buffer with carbon (GaN:C), which forms deep acceptors and pins the Fermi level deep in the bandgap.[1]

However, these deep carbon acceptors can trap charges for extended periods of time.[2–4] It has been demonstrated that the times for trapping as well as detrapping are ultimately limited by the conduction through GaN:C instead of the actual trapping and detrapping event.[3] As a result, not only the leakage current itself but also the trapping dynamics are determined by the leakage

current. Both charge trapping and leakage current can be detrimental to the performance and reliability of GaN HEMTs.[1–8]

Due to the lattice mismatch of the heteroepitaxy of GaN, especially on foreign substrates such as Si, dislocations are inherently present. For GaN-on-Si, dislocation densities are in the range of $10^9\,\mathrm{cm}^{-2}$. Dislocations are extended defects in the crystal lattice and are considered to have a major impact on the leakage current[3,8–22] and, hence, should also affect the trapping dynamics. One promising candidate that could explain this phenomenon is the carbon defect band model postulated by Koller *et al.*[23] According to this model, charges propagate within GaN:C in a defect band within the bandgap and not via the valence nor conduction band. The conductivity within this defect band correlates with the carbon concentration,[3] indicating that charges move directly between carbon defects. Koller *et al.* speculated that the average carbon concentration is not sufficient to have a homogeneous conduction mechanism in the entire matrix.[9,24] Instead, carbon has been hypothesized to accumulate in larger densities in the vicinity of certain dislocations and that conduction in these regions is enhanced. However, this hypothesis has never been verified by physical characterization.

Numerous studies have widely discussed possible root causes regarding the electrical activity of a dislocation. Previously, threading dislocations with a pure screw component, also referred to as threading screw dislocations (TSDs), were believed to be the culprit of localized conductivity.[13,18,19,21] In addition to dislocation types, other determining factors of electrically active dislocations may include their imposed strain fields,[16,18,25–27] the absolute magnitude of the Burgers vector,[12,16,28] the angular orientation of the dislocation vector lines,[11] and the difference in growth stoichiometry at the dislocation relating to local chemical and structural, as well as electronic property changes.[10,15,17,18,20,29,30]

Other research groups have suggested that not the strain field itself but the segregation of impurities due to the dislocation-induced strain fields could be a cause of enhanced leakage current.[16,26,28,29,31] In addition to a report of excess Mg impurities at the core of dislocations,[14] several publications have reported oxygen impurities,[20,29,31,32] excess gallium accumulation,[18,19] or a lack of nitrogen atoms[27] as other contributors to leakage current in GaN.

B. Novel approach to study dislocations in GaN

Until now, the electrical behavior of dislocations has been investigated in various GaN layers such as the AlGaN barrier, p-doped, n-doped, and unintentionally doped GaN (GaN:uid), but never in carbon-doped GaN. However, due to the role of GaN:C as an insulating layer, the electrical behavior within this layer is of considerable importance. To date, no studies have compared the leakage current at dislocations in GaN:C nor have any investigated their chemical composition.

One major reason is that in standard HEMT stacks, the GaN:C layer is buried deep below the surface.[28,33] This (1) does not allow for electrical characterization with a lateral resolution that is required in order to study individual dislocations and (2) does not allow for top-down view dislocation localization with techniques such as atomic force microscopy (AFM), electron channeling contrast imaging (ECCI), as well as all other electron beam based techniques. Although subsequent cross-sectional analysis could address the second point, it would require considerably more effort. The first point, however, poses an unsolvable obstacle in HEMT structures and requires special test structures.

To overcome this obstacle, some of the co-authors have introduced test structures featuring a GaN:C/nGaN bilayer with nGaN being silicon doped n-type GaN. These structures allow for the electrical characterization of single GaN:C layers.[1] In a recently published study,[33] it was demonstrated that these structures can be utilized for electron beam induced current (EBIC) measurements, enabling the identification of electrically active regions. Following this, ECCI analysis allows for the correlation of active regions with dislocations, which can then be encapsulated in a transmission electron microscopy (TEM) lamella for further TEM-based analyses.

While previous electron energy loss spectrometry (EELS) studies[34,35] have identified oxygen segregation in dislocations,[29,32] no research has yet correlated their measured electrical behavior with TEM studies on conductive dislocations, especially within carbon-doped GaN.

C. Our research objective

The objective of our investigation is to study the connection between the electrical activity of a dislocation and the elemental composition of that specific dislocation and its surroundings in carbon-doped GaN. On the basis of this approach, we demonstrate that electrically active dislocations in the semi-insulating GaN:C layer can be distinctly identified using two different electrical pre-characterization techniques: conductive atomic force microscopy (C-AFM) and EBIC. Subsequently, we analyzed their chemical composition through EELS with a focus on carbon.

Section II describes the investigated GaN:C samples and the analytical techniques that were used to characterize them.

In Sec. III, we examine the correspondence between electrically active dislocations and their chemical composition in terms of segregated carbon impurities. We compare these results with first-principles total-energy calculations done within the density functional theory (DFT) for carbon at threading $a+c$ mixed type dislocations in GaN, where a and c are the Burgers vector components with $a = (1/3)\langle 11\bar{2}0\rangle$ and $c = \langle 0001\rangle$. Finally, we discuss how an enhanced carbon concentration in the vicinity of dislocations can influence electronic properties such as the vertical leakage current.

II. EXPERIMENTAL DETAILS

A. Samples

Two GaN:C/nGaN bilayer test structures grown on a 6 in. p-doped Si(111) substrate via metal organic chemical vapor deposition are investigated in this study, referred to as S50 and S80, as seen in Fig. 1. S50 consists of a 40 nm thick GaN:C buffer layer and a 10 nm thick GaN:uid layer, on top of a 1 μm layer of nGaN, transition layers, and the Si(111) substrate. S80 comprises an 80 nm thick GaN:C buffer layer on top of a 1.7 μm thick nGaN layer, transition layers, and the Si(111) substrate. Both samples have an estimated carbon concentration of approximately $10^{19}\,\mathrm{cm}^{-3}$ in the

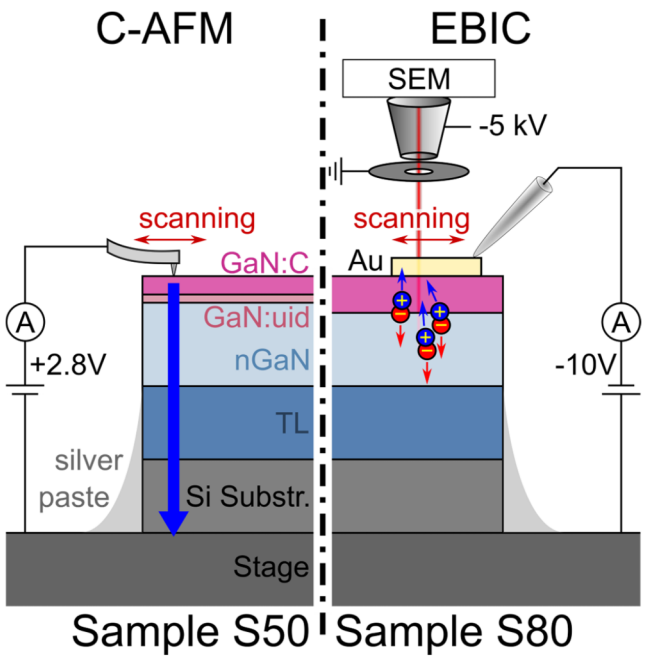

FIG. 1. Investigated GaN:C/nGaN bilayer test structures: S50 (left) and S80 (right). S50 has a 40 nm GaN:C buffer layer with 10 nm GaN:uid on top of 1 μm of nGaN, transition layers, and the Si(111) substrate. S80 is made of an 80 nm GaN:C buffer layer with 1.7 μm nGaN on top of transition layers and the Si(111) substrate. Sample S50 is optimized for use in C-AFM, while S80 is optimized for EBIC analysis.

GaN:C buffer layer with an active donor concentration N_d of 8.5×10^{16} cm^{-3} in the nGaN layer. Further details on electrical characterization of these GaN:C/nGaN bilayers can be found in Koller *et al.*[1]

The epitaxial structures and contacts utilized in this study differ significantly from commercially available devices and are employed exclusively for research.

B. Methods

C-AFM measurements were performed in a Park Systems NX20 AFM system. Using a single-crystal diamond probe highly doped with boron (Adama Apex Super Sharp AFM), it is possible to achieve an effective probe radius <5 nm. The cantilever AD-2.8-SS system uses a spring constant of 2.8 N/m.

The EBIC measurement setup utilized a Zeiss Supra 55 scanning electron microscope (SEM), a Kleindiek Nanotechnik LT6620 stage with Zyvex dProber nanomanipulators, in addition to a Keithley 2400 source measure unit meant to apply bias and measure the electron beam induced current.

A TESCAN S9000G dual-beam focused ion beam (FIB) and SEM was used to create markers via focused electron beam induced deposition and to create the lamellae for scanning transmission electron microscopy (STEM) EELS investigations. Additionally, a Helios Hydra dual-beam FIB and SEM was used to manufacture further samples for STEM EELS.

We performed all TEM analysis on an FEI Tecnai F20 (S)TEM capable of varying the electron beam energy from 60 to 200 keV and possessing a probe size of <2 nm in STEM mode. EELS measurements were analyzed through a Gatan GIF Tridiem energy filter. Core-loss EELS measurements include the ionization edges of carbon at 284 eV, nitrogen at 401 eV, and oxygen at 532 eV. Measurements of the electron energy loss near edge structure (ELNES) are used to determine the differences in the electronic nature of carbon at the dislocation core compared to carbon in the GaN:C matrix.[36,37] We further performed statistical multivariate analysis such as principal component analysis (PCA) to reduce statistical noise from the acquired EELS spectra.

To investigate the interaction between $a+c$ mixed type dislocations and C substitutionals in GaN, we employ DFT calculations within the local density approximation (LDA) and the projector augmented-wave (PAW) method.[38,39] The Ga d electrons are included as valence states, and a plane wave energy cutoff of 450 eV was used. To model undissociated $a+c$ mixed type dislocations, we used supercells with periodic boundary conditions. Each supercell contains a nanowire (NW) of the hexagonal cross section with its axis oriented along [0001] and bounded by m-plane facets [as seen later in Fig. 7(a)]. The Ga and N dangling bonds at the facets are passivated by partially charged pseudohydrogen that obey the electron counting rule. The dislocation line coincides with the axis of the nanowire, the atoms are displaced from their bulk-like position according to elasticity theory.[40] To decouple the NWs from their periodic images, a vacuum with thickness of 15 Å is used. Furthermore, the thicknesses of the supercell along the c-axis are two lattice constants, i.e., four GaN monolayers, and the NW diameter is ≈36 Å. The supercells consist of 1060 atoms. The Ga and N atoms in an outershell of a double monolayer thickness were kept fixed to the positions defined by elasticity theory. All other Ga and N atoms are relaxed until the change in the total energy is less than 10^{-5} eV.

To calculate the chemical potential of the charge neutral C substitutionals, we substituted Ga and N atoms with C at selected sites outside the core region in both the compressive and tensile regions of the dislocations. As the reference for the C chemical potential, we used the calculated chemical potential of the C substitutional in a $5 \times 3 \times 3$ orthogonal bulk cell consisting of 360 atoms.

III. RESULTS AND DISCUSSION

A. Revealing electrically active regions in GaN:C

1. Conductive atomic force microscopy (C-AFM)

We employ C-AFM to map areas with enhanced leakage current, while simultaneous AFM measurements show the topography including pits at dislocations. Therefore, as schematically illustrated on the left side of Fig. 1, the needle is grounded and the chuck is set to a negative bias.

In general, the investigated structures behave similar to a diode, whereby the dislocation-free bulk and non-active dislocations show higher forward voltage (V_F) than active dislocations. In a first step, we evaluate the V_F of the bulk and then stay with the

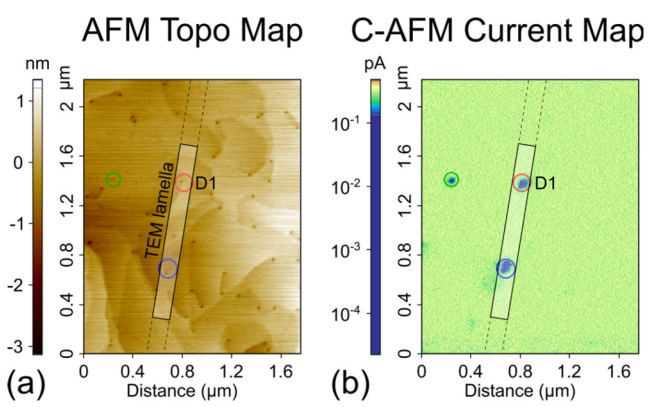

FIG. 2. (a) AFM surface topography and (b) simultaneously recorded C-AFM vertical leakage current mapping using a bias of 2.8 V.

bias below this value so that in C-AFM, only the active dislocations conduct current.

Figure 2 compares the AFM surface topography in (a) with its C-AFM vertical leakage current mapping in (b). Note that the isolated spots of vertical leakage current coincide one-to-one with particular dislocations. We specifically did not choose ambiguous spots, which could potentially correlate with multiple dislocations. The highlighted box in Fig. 2 schematically shows part of the afterward extracted TEM lamella. D1 indicates the electrically active dislocation that corresponds with the isolated leakage current spot in the C-AFM current map.

2. Electron beam induced current (EBIC)

For EBIC analyses, 20 nm thick, 100 μm diameter sized semi-transparent ohmic Ti/Au top contacts are deposited. This electrode is contacted via a nanoprobe needle biased to −10 V and the chuck is set to ground. Leakage current is confined within the GaN:C layer beneath the metal contact, whereas it laterally distributes in nGaN over the entire sample, rendering the impedance of the bottom layers under nGaN negligible. As schematically illustrated on the right side of Fig. 1, for EBIC analysis an electron beam penetrates through the semi-transparent contact into the reverse biased GaN:C/nGaN bilayer. Using an electron beam voltage of 5 kV, electrons propagate approximately 200 nm into the sample and generate electron–hole pairs within this volume. Internal electric fields separate electrons and holes, and let them propagate to the anode and cathode, respectively. This is measured as current, giving this technique its commonly used name "electron beam induced current." In previous publications,[24,33] we described in more detail how local variations in resistivity as well as the trapping behavior, e.g., due to higher defect densities, can alter the measured current and result in locally enhanced currents. In the following, we refer to these regions with enhanced current as "EBIC spots" or "electrically active regions."

Figure 3 depicts an ECCI map on the left and an EBIC current map with EBIC spots of the same region on the right. All

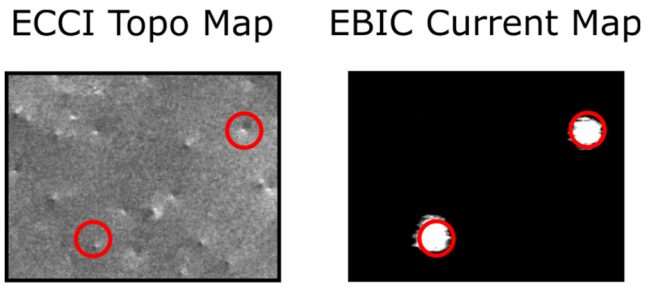

FIG. 3. Comparison of an ECCI surface topography map with an EBIC map of the same region. We see one-to-one correlation between EBIC spots and dislocations.

black-white points in ECCI originate from dislocations.[41,42] Direct comparison of EBIC and ECCI reveals a one-to-one correspondence of the EBIC spots with single dislocations in ECCI. Analogous to the cantilever-based techniques where only a few dislocations caused enhanced current in C-AFM, also only a few dislocations observed in ECCI lead to EBIC spots. Similar to C-AFM/AFM, we only chose EBIC spots that could unambiguously be correlated with a single dislocation.

B. Carbon segregation at dislocations

In order to determine the chemical composition of dislocations, we employ EELS. With our setup, a detection limit of approximately 1% can be achieved, although quantitative values could not be extracted due to the lack of a proper reference.

Figures 4(a) and 4(b) show the cross correlation of dislocations in top-down view measured by AFM surface topography with dislocations in the cross-sectional view imaged by STEM. The highlighted box in Fig. 2 indicates the position of the cross-sectional TEM lamella in Fig. 4(b). We obtain a one-to-one correspondence confirming that the dislocation of interest has been encapsulated and extracted in the TEM lamella. We measured 32 different positions across samples S50 and S80; however, due to the challenges of sample preparations, six electrically active dislocations could be encapsulated in 70–180 nm thick lamellae for TEM analysis. In this study, we focus in particular on two electrically active dislocations: one determined by C-AFM in sample S50 and one determined by EBIC in sample S80.

Besides EELS, we employed TEM two beam diffraction conditions. While the main image [Fig. 4(b)] shows a STEM high angle annular dark-field (HAADF) image, in the two insets on the right, certain diffraction conditions were applied that make dislocations with Burgers vector with $a = (1/3)\langle 11\bar{2}0\rangle$ and $c = \langle 0001\rangle$ component invisible [see Figs. 4(c) and 4(d), respectively]. The electrically active dislocation, marked with D1, is identified as a threading mixed type dislocation (TMD) as it is visible in both conditions. In contrast, the electrically inactive dislocation next to it, marked with D2, is only visible in the bottom inset and, therefore, identified as a threading edge type dislocation (TED).

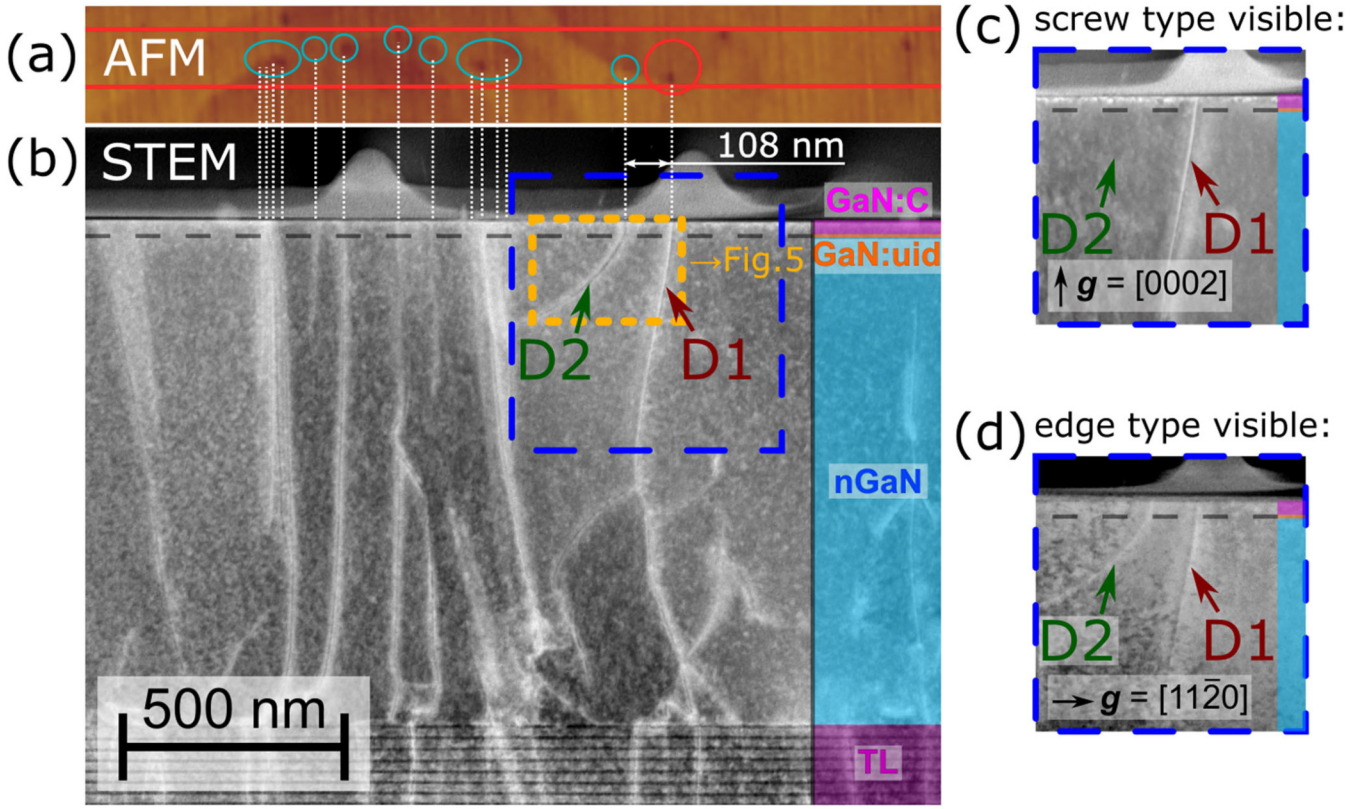

FIG. 4. Cross correlation of dislocations in (a) top-down view measured by AFM surface topography with (b) a cross-sectional view imaged by STEM. (c) and (d) show transmission electron microscopy (TEM) images in two beam diffraction conditions $\boldsymbol{g} = [0002]$ and $\boldsymbol{g} = [11\bar{2}0]$ for dislocation type determination, indicating that the C-AFM electrically active dislocation D1 is mixed type and the electrically inactive dislocation D2 is edge type.

While the six investigated electrically active dislocations were TMDs, the majority of TMDs do not lead to electrically active regions. Therefore, the Burgers vector by itself is not a sufficient indicator of whether a dislocation is electrically active or inactive.

Figure 5 examines the elemental analysis of electrically active and inactive dislocations, utilizing 200 keV STEM core-loss EELS measurements. Figures 5(a) and 5(b) are STEM HAADF images from the two case studies, where Fig. 5(a) displays the extracted C-AFM active dislocation, and Fig. 5(b) shows the extracted EBIC active dislocation. Figure 5(a) comes from the region indicated by the golden dashed box in Fig. 4(b). Figures 5(c) and 5(d) are the elemental maps of carbon using the carbon K-shell ionization edge (C-K edge) at 284 eV. Line scans (in orange) at the positions of the two different electrically active dislocations, D1 and E1, reveal for both significantly enhanced carbon in a region of approximately 20 nm around the core as seen in Figs. 5(e) and 5(f) in blue. An additional line scan of the electrically inactive dislocation from C-AFM marked as D2 is denoted with a green dotted line in Fig. 5(e) and also shows enhanced carbon concentration.

While all six active dislocations showed enhanced carbon consistently, out of the seven studied inactive dislocations, only two showed enhanced carbon. In Table I, this finding is summarized and interpreted as a Bernoulli process[43] (a series of Bernoulli trials, experiments with exactly two mutually exclusive outcomes, analogous to a coin-toss), with the observed absence (rather than presence) of excess carbon being used as random variable X: in n statistically independent trials on active and inactive dislocations, there are x cases of observed absence of carbon, where the probability of observing that outcome is given by the binomial distribution as

$$P(X = x; n,\ \theta) = \binom{n}{x}\theta^x(1-\theta)^{n-x}. \tag{1}$$

The most likely median and upper/lower confidence estimates for the corresponding probability θ of excess carbon being absent from a dislocation follow standard approaches: the maximum likelihood estimator is $\hat{\theta}_{\mathrm{ML}} = \frac{x}{n}$, whereas median and upper/lower single-sided 90% confidence estimates are the Clopper–Pearson values with $P(X \le x; \hat{\theta}_{\mathrm{med}}) = 0.5$, $P(X \le x; \hat{\theta}_{\mathrm{UCL}}) = 0.1$, $P(X \ge x; \hat{\theta}_{\mathrm{LCL}}) = 0.1$, respectively.[44,45]

Even by our admittedly low statistics of 0/6 carbon-free active dislocations and 5/7 carbon-free inactive dislocations, we can infer from the median estimate that C-absence in active dislocations is

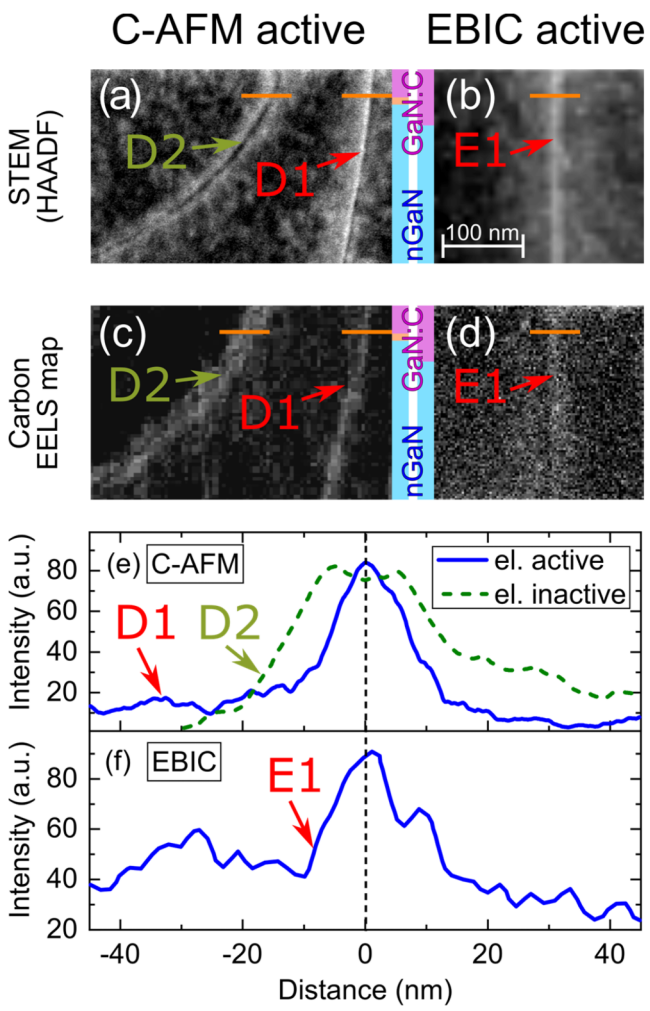

FIG. 5. (a) shows the STEM image of the region, marked by a golden dashed box in Fig. 4(b) encapsulating a dislocation (D1) that has been electrically active in C-AFM and one that has been electrically inactive (D2). (b) shows a STEM image of a dislocation that has been electrically active in EBIC. (c) and (d) show the corresponding carbon EELS maps. Line scans in (e) and (f) reveal that all three dislocations showed enhanced carbon concentrations in the vicinity of the dislocations. (c) and (d) show carbon enhancement even in the nGaN layer under GaN:C.

seven times less probable than in inactive dislocations. Conversely, electrically active dislocations typically are seven times more likely to contain segregated carbon than electrically non-active dislocations. The nonoverlapping 90% confidence bounds for active and inactive dislocations suggest that carbon segregation and electrical activity are, indeed, correlated. In addition, assuming irrelevance of carbon segregation regarding electrical activity by simply summing up all observations independent of electrical property in the last line of Table I would estimate 38% of dislocations to be carbon-free. Inserting this value of $\theta = 0.384$ into (1) yields a probability of only 5.5% for the 0/6 observation on active dislocations. Finally,

TABLE I. Summary of the investigation of 13 dislocations, classified by their electrical activity. The observed absence of excess carbon in their vicinity is the random variable of a Bernoulli process of n trials and x successes, with the underlying binomial distribution being parametrized by probability θ for excess carbon being absent from active or inactive dislocations. θ is estimated at maximum likelihood $\hat{\theta}_{ML}$, and by Clopper–Pearson values for upper and lower confidence estimates $\hat{\theta}_{UCL}$ and $\hat{\theta}_{LCL}$ and also for a median estimate $\hat{\theta}_{med}$.

	n	x	$\hat{\theta}_{ML}$	$\hat{\theta}_{med}$	$\hat{\theta}_{UCL}$	$\hat{\theta}_{LCL}$
Active	6	0	0	0.11	0.32	…
Inactive	7	5	0.71	0.77	0.92	0.40
All/irrelevant	13	5	0.38	0.43	0.59	0.20

the data can also be summarized in the form of a contingency table (Table II), where Fisher's exact test[44]—appropriate for small sample sizes—can be used to compute a probability for this observation to be obtained accidentally with the underlying hypothesis of carbon segregation being irrelevant to electrical activity. The value of $p = 0.0163$ discards the null hypothesis and proves the correlation to be >98% significant. Therefore, the authors dare formulating that carbon segregation is, indeed, a necessary (but clearly not sufficient) condition for the electrical activity of dislocations. A physical explanation for this statement shall be given in Sec. III D.

The elemental maps in Fig. 5 reveal that the change in the elemental composition in the vicinity of the dislocations is not just limited to the GaN:C layer. We notice that in the nGaN layer, even up to 200 nm below the GaN:C layer, the carbon enhancement exceeds the concentration of the GaN:C bulk. Furthermore, we observed that the EELS intensity of gallium remained unchanged; however, we noticed that in the vicinity of some dislocations, a dearth of nitrogen as well as an increase in the oxygen concentration was present. In the six electrically active dislocations and seven inactive dislocations, this was not consistent across all of them and no unambiguous correlation of oxygen and nitrogen with electrical activity of dislocations was found. Therefore, for the samples investigated within this study, we do not consider gallium, oxygen, and nitrogen as the determining factors for electrical activity.

In order to get more insights into the nature of the carbon atoms that accumulate at the electrically active dislocations, the electron energy loss near edge structure (ELNES) has been investigated. This technique reveals the density of unoccupied states above the Fermi level vs energy. ELNES, therefore, not only shows the

TABLE II. Investigations summarized in a contingency table, where Fisher's exact test may be used to assess the significance of the association between the classes of "carbon yes/no" and "active/inactive." Here, a p-value of 0.0163 indicates high statistical significance.

	Excess carbon found	No excess carbon found	Total dislocations investigated
Active	6	0	6
Inactive	2	5	7
All	8	5	13

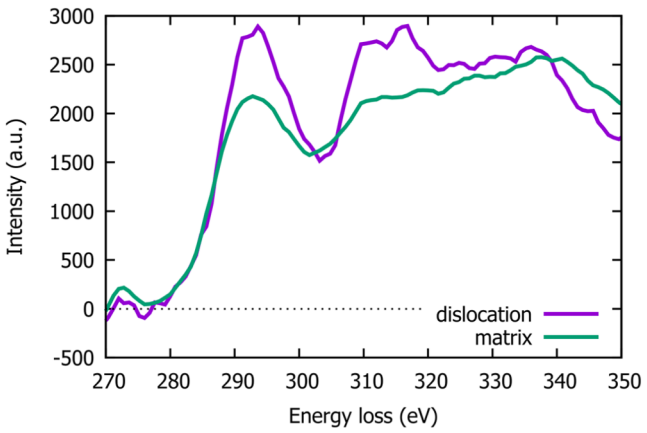

FIG. 6. EELS measurement of the fine structure of the carbon K-shell ionization edge (C-K edge) at around 284 eV of an electrically active dislocation compared to the bulk GaN matrix in the direct vicinity.

elemental atoms present but also gives insights into their binding configurations. For example, a carbon atom at a nitrogen site would have a different fingerprint than a carbon atom at a gallium site.

Figure 6 shows an EELS measurement of the fine structure of the ionization edges at around 284 eV, the C-K edge. The purple line represents the ELNES at an electrically active dislocation determined by C-AFM. The green line corresponds to the ELNES of the bulk GaN matrix adjacent to the dislocation. Distinct differences in the fine structure require different binding configurations of the carbon atoms in the GaN:C matrix and in the electrically active dislocation. More insights could be gathered by ELNES analyses of electrically inactive dislocations and comparison with density functional theory calculations. However, this was beyond the scope of this investigation.

C. Density functional theory (DFT) simulations

Figure 7(a) shows a schematic representation of the simulated supercell indicating the atomic positions for which chemical potentials are calculated. In Fig. 7(b), we plot the chemical potential $\Delta\mu_C$ of C_{Ga} and C_N at six different positions in the compressive and tensile strain fields of an $a+c$ mixed type dislocation. $\Delta\mu_C$ is calculated as

$$\Delta\mu_C = \mu_C - \mu_{C\,Bulk},$$

where μ_C and $\mu_{C\,Bulk}$ are the chemical potentials of C in the neighborhood of the dislocation and in the bulk-like material, respectively.

Both the tensile and compressive regions of the dislocation are attractive for C_N (C substituting for N). Moreover, our calculations indicate that besides a lattice site adjacent to the dislocation core, the compressive region is repulsive for C_{Ga} (C substituting for Ga). Nevertheless, the tensile region is strongly attractive. Previous DFT calculations have also revealed that the strain field of a *c*-type under the screw dislocation is attractive for Mg_{Ga} substitutionals.[15]

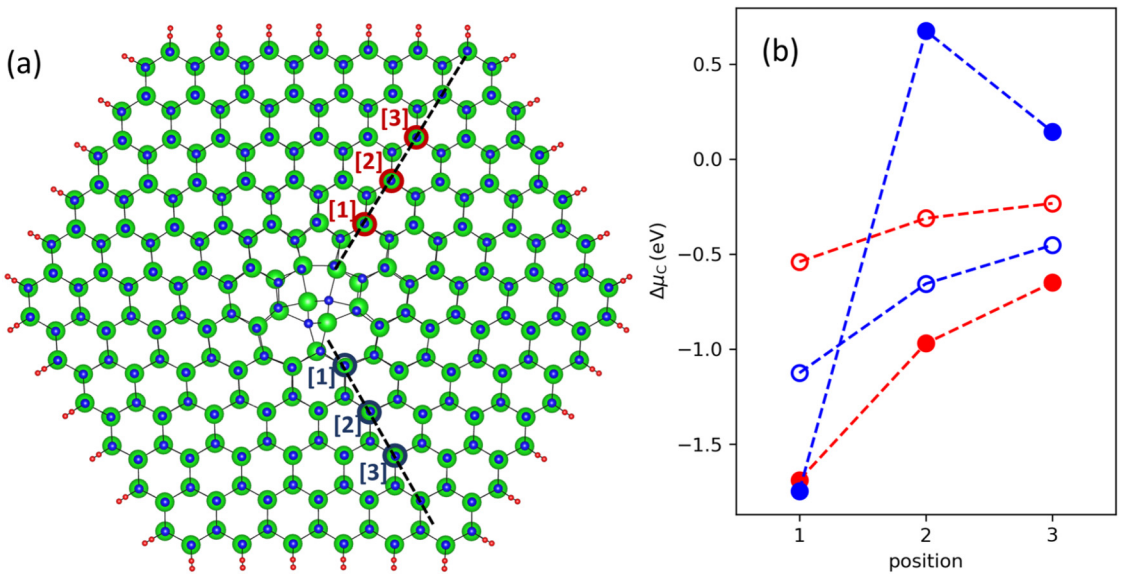

FIG. 7. (a) Schematic representation of an undissociated $a+c$ mixed type dislocation in GaN in top view. Large/green balls and small/blue balls indicate Ga and N atoms, respectively. Small/red balls are pseudohydrogens passivating the dangling bonds at the *m*-plane facets. The red and blue circles indicate the positions of C substitutionals in the tensile and compressive regions of the dislocation, respectively. (b) Calculated chemical potential of C_N (open circles) and C_{Ga} (filled disks) substitutionals. Blue and red symbols indicate the substitutionals in the compressive and tensile regions, respectively. The dashed line are guides to the eye. Position 1 is ≈6 Å away from the dislocation line. The distance between the other positions equals the lattice constant of GaN, i.e., it is equal to 3.15 Å.

The actual C content around a mixed type dislocation, under conditions of thermodynamic equilibrium, is governed by both the C chemical potential and the electrochemical potential, i.e., the position of the Fermi level. The value of the latter depends on the value of the former as well. To account for the relationship between the formation energy of carbon defects and the Fermi level, one must consider charged carbon defects within the strain field of the dislocation. However, this exceeds the scope of the present paper. Nevertheless, our calculations reveal a strong driving force for C substitutionals' segregation at mixed type dislocations in GaN. Moreover, the actual strain field is a superposition of the strain fields of nearby dislocations as well. This may alter the magnitude of the strain field, which, in turn, will affect the value of the chemical potential of charge neutral carbon substitutionals.

D. The role of carbon in electrically active dislocations

Previous studies[3] on GaN layers with carbon concentrations as low as 10^{18} cm^{-3} showed that charges propagated mainly via the valence band. When the carbon concentration exceeded 10^{19} cm^{-3}, the Fermi level effectively pinned at approximately 0.9 eV above the valence band maximum. The large distance to the valence band in contrast leads to insulating behavior in the higher carbon-doped layers. However, it was speculated that due to the high density of carbon defects, they form a resistive defect band within the bandgap.[23]

Koller *et al.*[24] proposed that most involved defects are carbon atoms at a nitrogen site, C_N, energetically approximately 0.9 eV above the valence band maximum, and that these defects accumulate preferentially at dislocations, as illustrated schematically in Fig. 8. They also speculate that only a few dislocations show significantly enhanced conductivity, while the majority do not. The conductivity of the defect bands has been observed to correlate with the overall carbon concentration.[3]

EELS analysis within this study confirms the speculated enhanced carbon concentration at dislocations. However, inactive dislocations also revealed enhanced carbon concentrations, suggesting that high concentration is not sufficient to cause dislocations to become electrically active. In the following, we propose possible mechanisms about the underlying reasons:

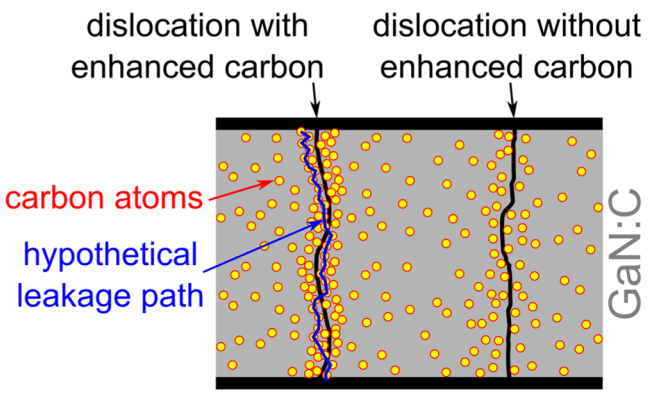

FIG. 8. Hypothetical carbon defect band model.

- *Carbon could be irrelevant:* While all electrically active dislocations showed enhanced carbon concentrations, it could be that the carbon content is not the underlying reason for electrical activity. Instead, both enhanced carbon concentration and electrical activity could originate from a different root cause.
- *Enhanced carbon concentration in nGaN:* In EBIC, the GaN:C/nGaN bilayer is reverse biased and especially after electron beam exposure, a significant part of the potential drops in nGaN. In pGaN/nGaN junctions, the diffusion of Mg from the pGaN region into the nGaN region leads to altered leakage current in these structures.[10] Similar to the idea of Mg diffusion through dislocation cores, we hypothesize that carbon could also diffuse along efficient paths via dislocation cores deep into nGaN. However, we would expect that (1) a large increase in the carbon concentration would make nGaN semi-insulating, while (2) a smaller increase in the carbon concentration would reduce the effective n-doping concentration and, consequently, reduce the electric fields in nGaN as well as in GaN:C. Both cases should result in a reduction in the current. Furthermore, for C-AFM, the GaN:C/nGaN bilayer is forward biased. Consequently, the main part of the potential drops in GaN:C, while the nGaN layer is not expected to play a significant role. All these aspects strongly suggest that the enhanced carbon concentration in nGaN is not the root cause for the observed higher currents at the electrically active dislocations. However, for other epitaxial stacks, this effect could be relevant, whereby it depends on the structure and whether it increases or decreases currents.
- *Shift of the C_N energy:* A previous DFT study on Mg doped GaN[15] revealed that the energy level of Mg dopants shifts at dislocations toward the conduction band. It has been speculated that while Mg doped GaN is usually p-type, it could switch at dislocations to n-type behavior. A similar effect could take place in GaN:C. The change in the energy level should strongly depend on the strain field, which is mainly determined by the Burgers vector. However, our study shows that dislocations with different Burgers vectors can be electrically active, and not all dislocations with the same Burgers vector are active. Hence, we consider that the Burgers vector is not the sole determining aspect for the electrical activity of a dislocation.
- *Interruption of the defect band:* Possibly, electrically active dislocations have a continuous, uninterrupted high carbon concentration throughout the entire GaN:C layer. In contrast, electrically inactive dislocations with high carbon concentrations could still have regions with low carbon concentrations that interrupt the conduction path.
- *Changes in the local donor-to-acceptor ratio* (DAR): In general, the conductivity in the defect bands not only depends on the total carbon concentration but also depends on the DAR. Previous studies[46,47] estimated DARs in GaN:C in the range of 0.5–0.7. We speculate that this ratio might be varying in the vicinity of dislocations. Changes in the DAR can have three major effects:

1. *Shift of the Fermi level:* For DARs close to 1 or even higher than 1, the Fermi level does not pin to the carbon acceptor at approximately 0.9 eV above the valence band maximum but shifts toward the conduction band, which can make GaN:C n-type. For semi-insulating behavior, DAR < 1 is critical, especially when the structure is biased.[46]
2. *Change in the defect band conductivity:* Conduction in the defect band is the highest for DAR = 0.5, while any deviations result in a decrease in the conductivity.[47]
3. *Change in C_N density:* The defect band conductivity is supposed to correlate with the density of C_N acceptors. However, carbon can also form carbon interstitials (C_i) and substitute gallium atoms (C_{Ga}), which are both donors. This could lead to a decrease in the C_N density and, therefore, to a less conductive defect band, even if the total carbon density is higher.

A change in the DAR affects the conductivity for the three aspects in different ways. For the first aspect—the shift of the Fermi level, a significant increase in the DAR can increase the conductivity. For the second aspect—the change in the defect band conductivity, the further the DAR deviates from 0.5, the lower the conductivity becomes. Dependent on the value of the unaltered DAR, a change in the DAR can lead to an increase or decrease in the conductivity. For the third aspect—the change in the C_N density, any increase in the DAR leads to a conductivity decrease.

A general statement in which way the DAR changes the conductivity cannot be made. It depends on various factors such as the electric field, temperature, adjacent layers, as well as the exact growth conditions. The growth conditions influence whether carbon forms acceptors or donors and, therefore, the unaltered DAR of the GaN matrix.[46] In addition, the densities of other defects such as oxygen, silicon, and hydrogen impurities as well as nitrogen vacancies affect the DAR. The observed enhanced oxygen concentration at dislocations as well as the lack of nitrogen can also influence the DAR and could explain the different electrical behavior of dislocations with enhanced carbon concentrations. Furthermore, the different ELNES fingerprints at the dislocation compared to the bulk suggest that carbon at electrically active dislocations forms different defects than carbon in the bulk.

IV. CONCLUSION

In this work, we could for the first time prove that electrically active dislocations in the insulating GaN:C layer are, indeed, carbon enriched. Electrical activity, i.e., locally enhanced electrical conductivity of dislocations, was identified by two physically different techniques: the needle-based C-AFM and the electron beam based EBIC technique. In both cases, carbon enrichment could be seen in STEM EELS, which strongly corroborates the generality of the statement that carbon enrichment at a dislocation line is a necessary prerequisite to its electrical activity. This finding aligns with the proposed conduction mechanism in GaN:C layers by Koller *et al.*, namely, the enrichment of carbon defects in the vicinity of dislocation lines. Moreover, in line with the experimental findings, DFT calculations reveal that the strain field of mixed type dislocations is attractive for C_N and C_{Ga} defects, although for C_{Ga}, this is relevant only for the tensile region of the strain field.

Even in electrically inactive dislocations, carbon enrichment was sometimes found (two out of seven cases, vs six out of six for electrically active dislocations). This means that carbon segregation alone is not a sufficient reason for a dislocation to become electrically active. The observed particularity of the C-K edge in the ELNES signal documented suggests that the type of defect carbon forms might be crucial for the electrical activity.

ACKNOWLEDGMENTS

The authors thank M. Reisinger and G. Pobegen for their valuable discussions and motivation to publish, as well as D. Tilly, T. Schinnerl, and A. Steiger-Thirsfeld for their experimental support. Z. F. Scales, M. Nelhiebel, and M. Stoeger-Pollach have received funds from the Austrian Research Promotion Agency (FFG, Project No. 905107). C. Koller and L. Lymperakis acknowledge the ALL2GaN Project (Grant Agreement No. 101111890) supported by the Chips Joint Undertaking and its members including the top-up funding by Austria, Belgium, Czech Republic, Denmark, Germany, Greece, the Netherlands, Norway, Slovakia, Spain, Sweden, and Switzerland.

AUTHOR DECLARATIONS

Conflict of Interest

The authors have no conflicts to disclose.

Author Contributions

Ze F. Scales: Conceptualization (lead); Data curation (lead); Formal analysis (lead); Investigation (lead); Methodology (lead); Software (equal); Validation (lead); Visualization (lead); Writing – original draft (lead); Writing – review & editing (lead). **Christian Koller:** Conceptualization (supporting); Data curation (supporting); Formal analysis (supporting); Funding acquisition (equal); Investigation (supporting); Methodology (supporting); Project administration (equal); Resources (equal); Software (supporting); Supervision (equal); Validation (supporting); Visualization (supporting); Writing – original draft (supporting); Writing – review & editing (supporting). **Liverios Lymperakis:** Conceptualization (supporting); Data curation (supporting); Formal analysis (supporting); Funding acquisition (equal); Investigation (supporting); Methodology (supporting); Project administration (supporting); Resources (supporting); Software (equal); Supervision (supporting); Validation (supporting); Visualization (supporting); Writing – original draft (supporting); Writing – review & editing (supporting). **Michael Nelhiebel:** Conceptualization (supporting); Funding acquisition (lead); Investigation (supporting); Methodology (supporting); Project administration (supporting); Supervision (supporting); Writing – review & editing (supporting). **Michael Stoeger-Pollach:** Conceptualization (supporting); Data curation (supporting); Formal analysis (supporting); Funding acquisition (equal); Investigation (supporting); Methodology (supporting); Project administration (equal); Resources (equal); Software (supporting); Supervision (lead); Validation (supporting); Visualization (supporting); Writing – original draft (supporting); Writing – review & editing (supporting).

DATA AVAILABILITY

The data that support the findings of this study are available from the corresponding author upon reasonable request.

REFERENCES

[1]C. Koller, G. Pobegen, C. Ostermaier, M. Huber, and D. Pogany, "The interplay of blocking properties with charge and potential redistribution in thin carbon-doped GaN on n-doped GaN layers," Appl. Phys. Lett. **111**(3), 032106 (2017).

[2]M. J. Uren, S. Karboyan, I. Chatterjee, A. Pooth, P. Moens, A. Banerjee, and M. Kuball, "'Leaky dielectric' model for the suppression of dynamic R_{on} in carbon-doped AlGaN/GaN HEMTs," IEEE Trans. Electron Devices **64**(7), 2826–2834 (2017).

[3]C. Koller, G. Pobegen, C. Ostermaier, and D. Pogany, "Effect of carbon doping on charging/discharging dynamics and leakage behavior of carbon-doped GaN," IEEE Trans. Electron Devices **65**(12), 5314–5321 (2018).

[4]M. J. Uren, M. Cäsar, M. A. Gajda, and M. Kuball, "Buffer transport mechanisms in intentionally carbon doped GaN heterojunction field effect transistors," Appl. Phys. Lett. **104**(26), 263505 (2014).

[5]M. J. Uren and M. Kuball, "Impact of carbon in the buffer on power switching GaN-on-Si and RF GaN-on-SiC HEMTs," Jpn. J. Appl. Phys. **60**(SB), SB0802 (2021).

[6]M. Meneghini, C. De Santi, I. Abid, M. Buffolo, M. Cioni, R. A. Khadar, L. Nela, N. Zagni, A. Chini, F. Medjdoub, G. Meneghesso, G. Verzellesi, E. Zanoni, and E. Matioli, "GaN-based power devices: Physics, reliability, and perspectives," J. Appl. Phys. **130**(18), 181101 (2021).

[7]G. Meneghesso, M. Meneghini, and E. Zanoni, in *Gallium Nitride-enabled High Frequency and High Efficiency Power Conversion* (Springer International Publishing, Cham, 2018).

[8]S. Besendörfer, E. Meissner, T. Zweipfennig, H. Yacoub, D. Fahle, H. Behmenburg, H. Kalisch, A. Vescan, J. Friedrich, and T. Erlbacher, "Interplay between C-doping, threading dislocations, breakdown, and leakage in GaN on Si HEMT structures," AIP Adv. **10**(4), 045028 (2020).

[9]C. Koller, G. Pobegen, C. Ostermaier, G. Hecke, R. Neumann, M. Holzbauer, G. Strasser, and D. Pogany, "Trap-related breakdown and filamentary conduction in carbon doped GaN," Phys. Status Solidi B **256**(6), 1800527 (2019).

[10]B. Rackauskas, S. Dalcanale, M. J. Uren, T. Kachi, and M. Kuball, "Leakage mechanisms in GaN-on-GaN vertical pn diodes," Appl. Phys. Lett. **112**(23), 233501 (2018).

[11]Y. Yao, Y. Ishikawa, M. Sudo, Y. Sugawara, and D. Yokoe, "Characterization of threading dislocations in GaN (0001) substrates by photoluminescence imaging, cathodoluminescence mapping and etch pits," J. Cryst. Growth **468**, 484–488 (2017).

[12]Y. Yao, Y. Sugawara, D. Yokoe, K. Sato, Y. Ishikawa, N. Okada, K. Tadatomo, M. Sudo, M. Kato, M. Miyoshi, and T. Egawa, "Correlation between structural properties and nonradiative recombination behaviors of threading dislocations in freestanding GaN substrates grown by hydride vapor phase epitaxy," CrystEngComm **22**(48), 8299–8312 (2020).

[13]S. Usami, Y. Ando, A. Tanaka, K. Nagamatsu, M. Deki, M. Kushimoto, S. Nitta, Y. Honda, H. Amano, Y. Sugawara, Y.-Z. Yao, and Y. Ishikawa, "Correlation between dislocations and leakage current of p-n diodes on a free-standing GaN substrate," Appl. Phys. Lett. **112**(18), 182106 (2018).

[14]S. Usami, N. Mayama, K. Toda, A. Tanaka, M. Deki, S. Nitta, Y. Honda, and H. Amano, "Direct evidence of Mg diffusion through threading mixed dislocations in GaN p–n diodes and its effect on reverse leakage current," Appl. Phys. Lett. **114**(23), 232105 (2019).

[15]T. Nakano, Y. Harashima, K. Chokawa, K. Shiraishi, A. Oshiyama, Y. Kangawa, S. Usami, N. Mayama, K. Toda, A. Tanaka, Y. Honda, and H. Amano, "Screw dislocation that converts p-type GaN to n-type: Microscopic study on Mg condensation and leakage current in p–n diodes," Appl. Phys. Lett. **117**(1), 012105 (2020).

[16]T. Hamachi, T. Tohei, M. Imanishi, Y. Mori, and A. Sakai, "Correlation between current leakage and structural properties of threading dislocations in GaN bulk single crystals grown using a Na-flux method," Jpn. J. Appl. Phys. **58**(SC), SCCB23 (2019).

[17]T. Hamachi, T. Tohei, Y. Hayashi, M. Imanishi, S. Usami, Y. Mori, and A. Sakai, "Comprehensive analysis of current leakage at individual screw and mixed threading dislocations in freestanding GaN substrates," Sci. Rep. **13**(1), 2436 (2023).

[18]J. W. P. Hsu, M. J. Manfra, D. V. Lang, S. Richter, S. N. G. Chu, A. M. Sergent, R. N. Kleiman, L. N. Pfeiffer, and R. J. Molnar, "Inhomogeneous spatial distribution of reverse bias leakage in GaN Schottky diodes," Appl. Phys. Lett. **78**(12), 1685–1687 (2001).

[19]J. W. P. Hsu, M. J. Manfra, R. J. Molnar, B. Heying, and J. S. Speck, "Direct imaging of reverse-bias leakage through pure screw dislocations in GaN films grown by molecular beam epitaxy on GaN templates," Appl. Phys. Lett. **81**(1), 79–81 (2002).

[20]B. Kim, D. Moon, K. Joo, S. Oh, Y. K. Lee, Y. Park, Y. Nanishi, and E. Yoon, "Investigation of leakage current paths in n-GaN by conductive atomic force microscopy," Appl. Phys. Lett. **104**(10), 102101 (2014).

[21]T. Narita, M. Kanechika, J. Kojima, H. Watanabe, T. Kondo, T. Uesugi, S. Yamaguchi, Y. Kimoto, K. Tomita, Y. Nagasato, S. Ikeda, M. Kosaki, T. Oka, and J. Suda, "Identification of type of threading dislocation causing reverse leakage in GaN p–n junctions after continuous forward current stress," Sci. Rep. **12**(1), 1458 (2022).

[22]J. S. Speck and S. J. Rosner, "The role of threading dislocations in the physical properties of GaN and its alloys," Physica B **273**, 24-32 (1999).

[23]C. Koller, G. Pobegen, C. Ostermaier, and D. Pogany, "Evidence of defect band in carbon-doped GaN controlling leakage current and trapping dynamics," in *2017 IEEE International Electron Devices Meeting IEDM* (IEEE, San Francisco, CA, 2017), pp. 33.4.1–33.4.4.

[24]C. Koller, "The role of carbon in creating insulating behavior in GaN-on-Si buffers: A physical model," Ph.D. dissertation (Technical University of Vienna, 2018).

[25]L. Lymperakis, J. Neugebauer, M. Albrecht, T. Remmele, and H. P. Strunk, "Strain induced deep electronic states around threading dislocations in GaN," Phys. Rev. Lett. **93**(19), 196401 (2004).

[26]I. Belabbas, M. A. Belkhir, Y. H. Lee, J. Chen, A. Béré, P. Ruterana, and G. Nouet, "Local electronic structure of threading screw dislocation in wurtzite GaN," Comput. Mater. Sci. **37**(3), 410–416 (2006).

[27]I. Belabbas, J. Chen, and G. Nouet, "Electronic structure and metallization effects at threading dislocation cores in GaN," Comput. Mater. Sci. **90**, 71–81 (2014).

[28]S. Besendörfer, E. Meissner, A. Lesnik, J. Friedrich, A. Dadgar, and T. Erlbacher, "Methodology for the investigation of threading dislocations as a source of vertical leakage in AlGaN/GaN-HEMT heterostructures for power devices," J. Appl. Phys. **125**(9), 095704 (2019).

[29]M. E. Hawkridge and D. Cherns, "Oxygen segregation to dislocations in GaN," Appl. Phys. Lett. **87**(22), 221903 (2005).

[30]Q. Chen, B. S. McKeon, S. Y. Zhang, F. Zhang, C. Hu, T. H. Gfroerer, M. W. Wanlass, D. J. Smith, and Y. Zhang, "Impact of individual structural defects in GaAs solar cells: A correlative and in operando investigation of signatures, structures, and effects," Adv. Opt. Mater. **9**(2), 2001487 (2021).

[31]J. Elsner, R. Jones, M. I. Heggie, P. K. Sitch, M. Haugk, T. Frauenheim, S. Öberg, and P. R. Briddon, "Deep acceptors trapped at threading-edge dislocations in GaN," Phys. Rev. B **58**(19), 12571–12574 (1998).

[32]I. Arslan and N. D. Browning, "Role of oxygen at screw dislocations in GaN," Phys. Rev. Lett. **91**(16), 165501 (2003).

[33]Z. F. Scales, C. Koller, S. Schoemann, M. Nelhiebel, M. Reisinger, J. Jatzkowski, P. Diehle, and M. Stoeger-Pollach, *Identifying Electrically Active Dislocations in GaN and the Challenge of Cross-correlative Physical Characterization* (ASM International, Phoenix, Arizona, 2023), pp. 469–477.

[34]I. Arslan, A. Bleloch, E. A. Stach, S. Ogut, and N. D. Browning, "Using EELS to observe composition and electronic structure variations at dislocation cores in GaN," Philos. Mag. **86**(29–31), 4727–4746 (2006).
[35]A. Gutiérrez-Sosa, U. Bangert, A. J. Harvey, C. Fall, and R. Jones, "Energy loss spectroscopy of dislocations in GaN and diamond: A comparison of experiment and calculations," Diamond Relat. Mater. **12**(3–7), 1108–1112 (2003).
[36]R. F. Egerton, *Electron Energy-loss Spectroscopy in the Electron Microscope* (Springer U.S., Boston, MA, 2011).
[37]H. L. Fraser, D. W. McComb, and R. E. A. Williams, "Transmission electron microscopy for physical metallurgists," in *Physical Metallurgy* (Elsevier, 2014), pp. 1143–1226.
[38]G. Kresse and J. Hafner, "*Ab initio* molecular dynamics for liquid metals," Phys. Rev. B **47**(1), 558–561 (1993).
[39]G. Kresse and J. Furthmüller, "Efficient iterative schemes for *ab initio* total-energy calculations using a plane-wave basis set," Phys. Rev. B **54**(16), 11169–11186 (1996).
[40]J. P. Hirth and J. Lothe, *Theory of Dislocations*, 1st edition (McGraw-Hill, New York, 1968).
[41]G. Naresh-Kumar, J. Bruckbauer, P. R. Edwards, S. Kraeusel, B. Hourahine, R. W. Martin, M. J. Kappers, M. A. Moram, S. Lovelock, R. A. Oliver, C. J. Humphreys, and C. Trager-Cowan, "Coincident electron channeling and cathodoluminescence studies of threading dislocations in GaN," Microsc. Microanal. **20**(1), 55–60 (2014).
[42]E. Pascal, B. Hourahine, G. Naresh-Kumar, K. Mingard, and C. Trager-Cowan, "Dislocation contrast in electron channelling contrast images as projections of strain-like components," Mater. Today Proc. **5**(6), 14652–14661 (2018).
[43]M. Dekking, *A Modern Introduction to Probability and Statistics: Understanding Why and How* (Springer, London, 2005).
[44]R. A. Fisher, *Statistical Methods and Scientific Inference* (Hafner Publishing Co., 1956).
[45]M. Thulin, "The cost of using exact confidence intervals for a binomial proportion," Electron. J. Stat. **8**(1), 817–840 (2014).
[46]C. Koller, L. Lymperakis, D. Pogany, G. Pobegen, and C. Ostermaier, "Mechanism leading to semi-insulating property of carbon-doped GaN: Analysis of donor acceptor ratio and method for its determination," J. Appl. Phys. **130**(18), 185702 (2021).
[47]B. Rackauskas, M. J. Uren, S. Stoffels, M. Zhao, S. Decoutere, and M. Kuball, "Determination of the self-compensation ratio of carbon in AlGaN for HEMTs," IEEE Trans. Electron Devices **65**(5), 1838–1842 (2018).